CHEMISTRY OF MATERIALS

pubs.acs.org/cm

Article

Sb^{3+} Dopant and Halogen Substitution Triggered Highly Efficient and Tunable Emission in Lead-Free Metal Halide Single Crystals

Yuyu Jing,[▽] Ying Liu,[▽] Xingxing Jiang, Maxim S. Molokeev, Zheshuai Lin, and Zhiguo Xia*

Cite This: *Chem. Mater.* 2020, 32, 5327−5334

Read Online

ACCESS | Metrics & More | Article Recommendations | Supporting Information

ABSTRACT: Rational doping and compositional control remain significant challenges in designing luminescent metal halides to achieve highly efficient and tunable emission. Here, the air-stable lead-free $Cs_2InCl_5·H_2O$ crystal with a zero-dimensional structure was investigated as a pristine compound to design new luminescence materials. Sb^{3+}-doping in $Cs_2InCl_5·H_2O:Sb^{3+}$ enabled broadband yellow emission with a photoluminescence quantum yield up to 95.5%. The emission colors can be expanded into the orange-red region by halogen compositional substitution for $Cs_2InX_5·H_2O:Sb^{3+}$ (X = Cl/Br/I). The optical characterizations along with the theoretical calculations demonstrate that the characteristic singlet and triplet self-trapped exciton emissions of ns^2-metal-halide centers account for the tunable luminescence. Moreover, the admirable stability against air and heat pave way for its further applications in white light-emitting diodes and high-resolution fluorescent signs in anti-counterfeiting technology. Our achievement in the case of Sb^{3+}-doped $Cs_2InCl_5·H_2O$ represents a successful strategy for developing stable lead-free metal halides with highly efficient emission for versatile optical applications.

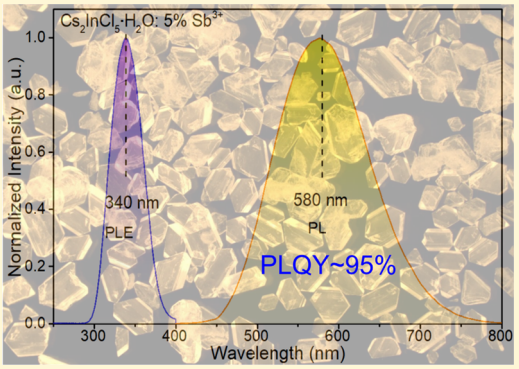

INTRODUCTION

All-inorganic three-dimensional (3D) lead halide perovskites $CsPbX_3$ (X = Cl, Br, I) have made remarkable progress in optoelectronic devices because of the near-unity photoluminescence (PL) quantum yield (PLQY) and facile synthetic procedure.[1−3] Nevertheless, the toxicity of lead (Pb) severely restricts further applications, which urges the public to search for environmentally amicable materials in this field. The feasible way is the replacement of Pb element by other nontoxic metal ions.[4,5] One of the mature substitution ways contains a cosubstitution of two Pb^{2+} with a monovalent ion and a trivalent ion.[6,7] Thus, 3D double perovskites $Cs_2M^+M^{3+}X_6$ (M^+ = Ag^+, Na^+; M^{3+} = Bi^{3+}, Sb^{3+}, In^{3+}; X = Cl, Br, I) have made extensive progresses.[8−11] Another tactic is the substitution of the trivalent metal element, such as Sb^{3+}, Bi^{3+}, forming $Cs_3M_2X_9$ with the zero-dimensional (0D) or two-dimensional layered crystal structure.[12,13] In addition, Sn-based perovskites (Cs_2SnX_6, $CsSnX_3$) and Cu-based perovskites ($Cs_3Cu_2X_5$, $CsCuX_3$) are also considered to be potential alternative materials in these years.[14−17]

Recently, low-dimensional metal halides have been the subject of focused interests owing to their unique soft lattice and the violent interaction of electrons with the lattice upon excitation, which results in the highly efficient broadband self-trapped excitons (STEs) emission.[18] Among lead-free 0D materials, In^{3+}-based compounds are rarely reported except for the structural characterization of $M_2[InCl_5(H_2O)]$ (M = K, Rb, Cs) and the recent study on $Cs_2InBr_5·H_2O$ with broad emission at 695 nm.[19−21] Furthermore, broadband emission with large Stokes shift is widespread for metal-halide perovskites, as found in the Cu-based system with intrinsic STEs emission and Na^+, Bi^{3+} codoped $Cs_2AgInCl_6$ with extrinsic STEs luminescence.[22−24] Generally, the emission energy of STEs is much smaller than the gap energy, leading to the large Stokes shift.[25] At present, rational ions doping is regarded as an efficient method to bring about extrinsic STEs emission.[26,27] Therefore, it is significant to unveil the underlying mechanism of extrinsic STEs, and thus one can find appropriate combination between the compounds and dopants to achieve efficient extrinsic STE luminescence.

Herein, a novel all-inorganic lead-free $Cs_2InCl_5·H_2O$ single crystal was discovered. $Cs_2InCl_5·H_2O$ possesses a unique 0D structure, and a broadband yellow emission has been achieved by introducing Sb^{3+} into this compound. Combined experimental studies by temperature-dependent PL spectra reveal that there exists a strong electron-phonon coupling resulting in the formation of STE emission with a near-unity PLQY of 95.5%. By halogen replacement from chlorine to iodine, PL

Received: April 22, 2020
Revised: May 15, 2020
Published: May 15, 2020

https://dx.doi.org/10.1021/acs.chemmater.0c01708
Chem. Mater. 2020, 32, 5327−5334

spectra of $Cs_2InX_5{\cdot}H_2O{:}Sb^{3+}$ crystals can be finely tuned from 580 to 660 nm. This work provides insights into the extrinsic STEs emission of Sb^{3+} as a dopant in 0D $Cs_2InCl_5{\cdot}H_2O$ and diverse applications including white light-emitting diodes (LEDs) and high-resolution fluorescent images for anticounterfeiting technology.

EXPERIMENTAL SECTION

Reagents. Cesium chloride (CsCl, 99.9%), Cesium bromide (CsBr, 99.9%), indium oxide (In_2O_3, 99.99%), antimony trioxide (Sb_2O_3, 99.9%), hydroiodic acid (HI, 55−58% in water by weight), and hydrobromic acid (HBr, 48% in water by weight) were purchased from Aladdin. Hydrochloric acid (HCl, 38% in water by weight) was purchased from Sinopharm Chemical Reagent Co., Ltd., China. All chemicals were used as received.

Synthesis. For $Cs_2InCl_5{\cdot}H_2O$ and Sb^{3+}-doped $Cs_2InCl_5{\cdot}H_2O$ crystals, CsCl (1 mmol), In_2O_3 (0.25 mmol) and Sb_2O_3 (0−0.05 mmol) were first dissolved in HCl at 110 °C for 10 min to form a clear solution. Then, the hot solution was transferred into a drying oven at 110 °C. Then, crystals were obtained by cooling the solution down to room temperature (RT) for 24 h. These obtained crystals were washed with ethanol three times and finally dried at 40 °C in an oven. For the synthesis of $Cs_2In(Cl/Br)_5{\cdot}H_2O{:}Sb^{3+}$ and $Cs_2In(Br/I)_5{\cdot}H_2O{:}Sb^{3+}$, HBr:HI aqueous solutions with designed compositions were used and the other conditions were kept invariable to obtain the corresponding crystals.

Characterization. The powder X-ray diffraction (XRD) patterns were measured using an Aeris powder diffractometer (PANalytical Corporation, using Cu Kα radiation at λ = 1.5406 Å, operating at 40 kV and 15 mA) at RT. Rietveld refinements were performed to analyze the crystal structures. The PL excitation (PLE)/emission spectra and the decay curves were measured by FLSP920 fluorescence spectrophotometer (Edinburgh Instruments Ltd., U. K.). The temperature-dependent spectra were measured by a Hitachi F-4600 fluorescence spectrophotometer with a heating apparatus and a 150 W Xe lamp as the excitation source. The PLQYs were measured on the FLS1000 instrument with the integrating sphere and white $BaSO_4$ powder was used as a reference to measure the absorption. The UV−vis absorption spectra were measured using the Hitachi UH4150 US−vis−near-infrared spectrophotometer at RT. The power density-dependent PL spectra were measured using the 375 nm (LE-LS-375-140TFCA, 1−140 mW) laser. Thermogravimetric analysis (TGA) were performed on TGA Q5000IR at 10 °C min^{-1} in a nitrogen flow from RT to 800 °C. Fourier transform infrared (FTIR) spectroscopy was measured by using the VERTEX 70 at RT. The (white LED) WLED was fabricated using a 365 nm chip, a blue-light emitter $BaMgAl_{10}O_{17}{:}Eu^{2+}$, and as-prepared yellow emitter $Cs_2InCl_5{\cdot}H_2O{:}Sb^{3+}$. The proper amounts of phosphors were thoroughly mixed with epoxy resin, and the obtained mixtures were coated on the LED chip. The photoelectric properties, including the emission spectra, correlated color temperature (CCT), color rendering index (R_a), and CIE color coordinates of WLEDs were measured using an integrating sphere spectroradiometer system (ATA100, Everfine).

Computational Methods. The first-principle calculation was performed by CASTEP with the planewave pseudopotential density functional theory (DFT).[28] The exchange−correlation term in Hamiltonian was described by Ceperley, Alder, Perdew, and Zunger (CA-PZ) in the form of local density approximation.[29] The optimized norm-conserved pseudopotential were used to deal with the interaction between the atomic cores and the valence electrons. This enables us to adopt a relatively small plane wave bases without affecting the accuracy of the calculation. The kinetic energy cutoff value was 900 eV, and the Monkhorst Pack k-point grid with density less than 0.04/Å^3 was selected.

RESULTS AND DISCUSSION

$Cs_2InCl_5{\cdot}H_2O$ single crystals were obtained from slowly cooling hydrochloric acid solution by reacting In_2O_3 and CsCl. Pure $Cs_2InCl_5{\cdot}H_2O$ phase was confirmed by XRD analysis with the space group *Pnma* [cell parameters: a = 14.4273(4) Å, b = 10.3915(2) Å, c = 7.4177(2) Å]. In this structure, each In atom is coordinated with five Cl atoms and one O atom from coordinating water to form an $InCl_5O$ structural unit. Every $InCl_5O$ unit is separated by two Cs^+ ions to create a 0D structure, as shown in Figure 1a. A distinct separation among individual $InCl_5O$ octahedrons is shown in Figure 1b. Sb^{3+}-doped $Cs_2InCl_5{\cdot}H_2O$ crystals were synthesized

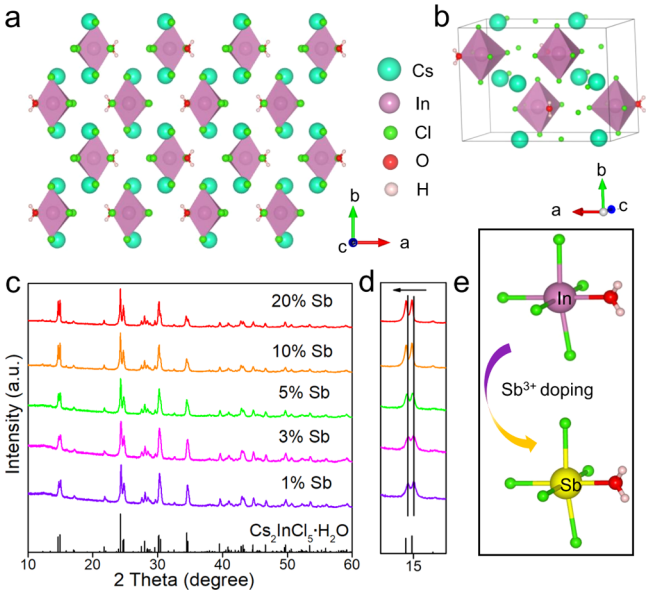

Figure 1. (a) Crystal Structure diagram of $Cs_2InCl_5{\cdot}H_2O$. (b) View of the individual $InCl_5O$ octahedral unit separated by Cs^+ ions full-range (c) and selected range (d) of the powder XRD patterns of Sb^{3+}-doped $Cs_2InCl_5{\cdot}H_2O$ powders with Sb^{3+} amount from 1% to 20%. Standard diffraction patterns of $Cs_2InCl_5{\cdot}H_2O$. (e) Schematic diagram demonstrating the Sb^{3+} substitution process.

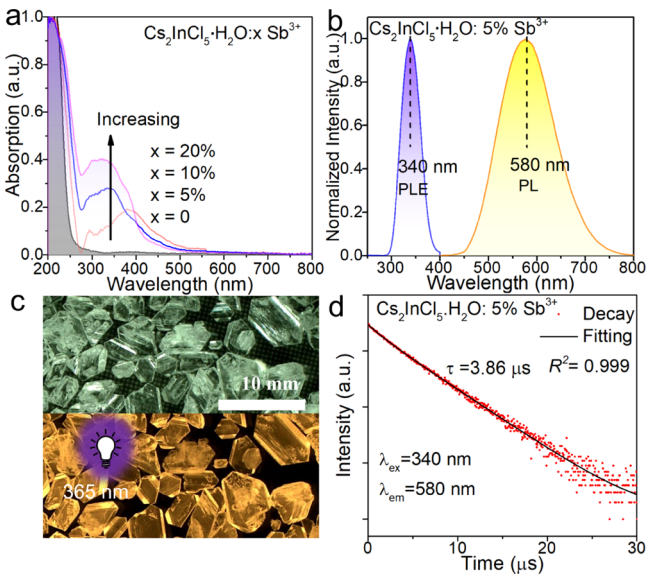

Figure 2. (a) UV−vis absorption spectra of $Cs_2InCl_5{\cdot}H_2O{:}xSb^{3+}$ (b) PLE (with monitoring wavelength at 580 nm) and PL (with excitation wavelength at 340 nm) spectra of as-prepared $Cs_2InCl_5{\cdot}H_2O{:}5\%\ Sb^{3+}$ (c) Photographs of $Cs_2InCl_5{\cdot}H_2O{:}5\%\ Sb^{3+}$ single crystals under natural light (top) and UV light (bottom). (d) Time-resolved PL spectra of $Cs_2InCl_5{\cdot}H_2O{:}5\%\ Sb^{3+}$.

https://dx.doi.org/10.1021/acs.chemmater.0c01708
Chem. Mater. 2020, 32, 5327−5334

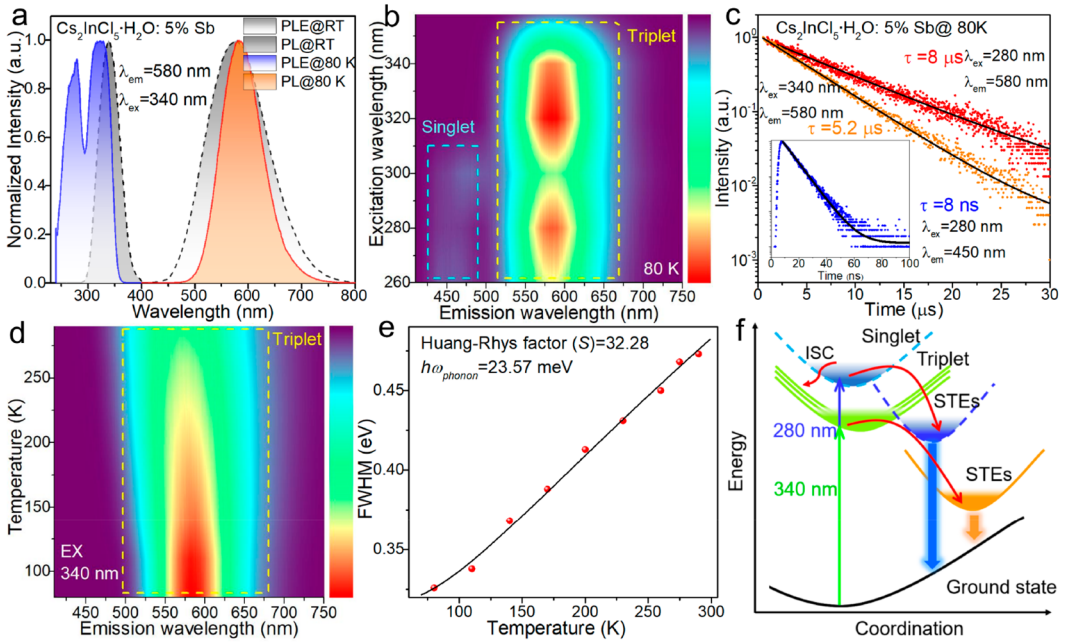

Figure 3. (a) PLE and PL spectra of $Cs_2InCl_5·H_2O$:5% Sb^{3+} at RT and 80 K. (b) PL/PLE correlation maps of $Cs_2InCl_5·H_2O$:5% Sb^{3+} measured at 80 K. (c) Time-resolved PL spectra of $Cs_2InCl_5·H_2O$:5% Sb^{3+} at 80 K excited by 280 nm and 340 nm. (d) PL/temperature correlation maps of $Cs_2InCl_5·H_2O$:5% Sb^{3+} upon excitation at 340 nm, along with temperature change from 80 to 290 K. (e) fwhm of the PL spectra as a function of temperature. Data are fitted by eq 2 (f) Schematic illustration of the recombination mechanism in $Cs_2InCl_5·H_2O$:Sb^{3+}.

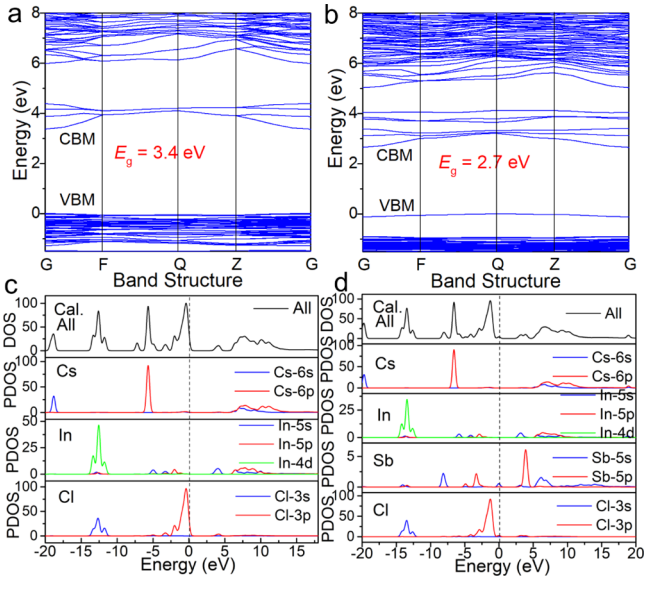

Figure 4. (a,b) Band structures of $Cs_2InCl_5·H_2O$ and the Sb^{3+} doped $Cs_2InCl_5·H_2O$ calculated with the DFT method. (c,d) Total and partial density of states of $Cs_2InCl_5·H_2O$ and Sb^{3+}-doped $Cs_2InCl_5·H_2O$ based on the DFT method.

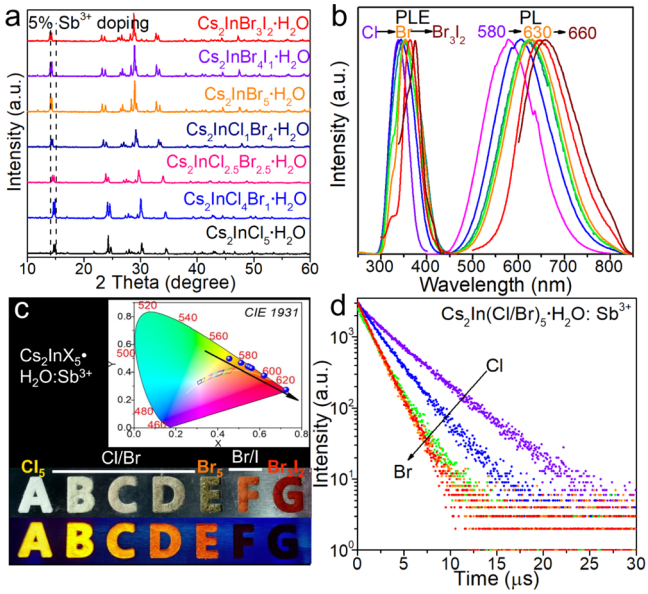

Figure 5. (a) Powder XRD patterns of Sb^{3+}-doped $Cs_2InX_5·H_2O$ (X = Cl/Br/I) depending on different halogen compositions. (b) PLE and PL spectra of $Cs_2InX_5·H_2O$:Sb^{3+} (X = Cl/Br/I) (c) CIE coordinates and the corresponding crystal powder photograph of $Cs_2InX_5·H_2O$:Sb^{3+} (X = Cl/Br/I) under natural light (top) and UV light (bottom). (d) TRPL spectra of $Cs_2InX_5·H_2O$:Sb^{3+}, where X stands for Cl, Br, and mixed halogen.

via the same synthesis procedure and the XRD patterns are given in Figure 1c. Moreover, the Rietveld refinement is performed using program TOPAS 4.2 to analyze the detailed structural evolution.[30] Obviously, all samples match well with the standard diffraction pattern. As shown in Figure 1d, the XRD peaks of Sb^{3+}-doping samples moved toward lower diffraction degrees as the concentration of Sb^{3+} increased. Moreover, all the XRD refinements with low R-factors demonstrated that the cell volume expanded gradually as summarized in Table S1. The cause may be that the polarity of the covalent bond decreases after the substitution of Sb^{3+} from 1.38 (In−Cl) to 1.11 (Sb−Cl) based on Pauling electronegativity scale (Figure 1e).

Furthermore, the DFT calculations were carried out to investigate the formation energy of Sb^{3+} in $Cs_2InCl_5·H_2O$. The formation energy (E) can be used to judge the occupancy site

https://dx.doi.org/10.1021/acs.chemmater.0c01708
Chem. Mater. 2020, 32, 5327−5334

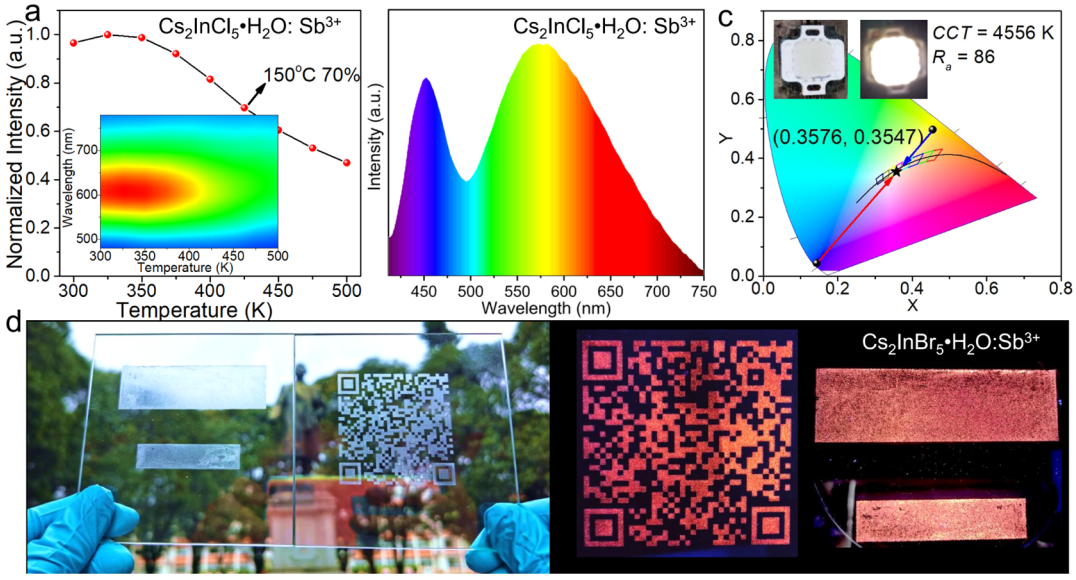

Figure 6. (a) PL intensity of $Cs_2InCl_5·H_2O:Sb^{3+}$ as a function of temperature in the range of 300−500 K. The inset shows the PL/temperature correlation maps of $Cs_2InCl_5·H_2O:Sb^{3+}$. (b) PL spectra of the NUV-pumped WLED based on $Cs_2InCl_5·H_2O:Sb^{3+}$ at 20 mA drive current (c) CIE coordinates of the NUV-pumped WLED. The inset shows photographs of WLED with power off and on. (d) Intricate images (such as QR codes) of $Cs_2InBr_5·H_2O:Sb^{3+}$ obtained by screen printing, and the corresponding emission can be checked clearly.

of the Sb^{3+} ion. The energy is given by the following equations[31]

$$E(Sb_{In}) = E(doped) - E(pure) - u_{Sb} + u_{In} \quad (1)$$

$$E(Sb_i) = E(doped) - E(pure) - u_{Sb} \quad (2)$$

where E(doped) and E(pure) are the total energies of the Sb^{3+}-doped system and perfect system, and the chemical potentials u_{Sb} and u_{In} are denoted as the Sb and In atoms, respectively. The calculation results reveal that the formation energy of Sb_i is much higher than that of Sb_{In} (1358.003 eV ≫ 3.225 eV), indicating that the replacement process is more energetically favorable than insertion in the cavity. Further evidence of component analysis via X-ray photoelectron spectroscopy (XPS) spectrum measurements (Figure S1) show the characteristic peaks for Cs, In, Sb, and Cl. There are two peaks that locate at 532.5 and 540.0 eV belonging to Sb^{3+} ions that authenticate the successful Sb^{3+} doping.[32]

The optical properties of the $Cs_2InCl_5·H_2O:Sb^{3+}$ powder were studied by the UV−vis absorption spectrum and PL spectroscopy, respectively. As shown in Figure 2a, the pristine $Cs_2InCl_5·H_2O$ shows an abrupt absorption edge at 250 nm (4.96 eV). While, an additional absorption peak appears at ∼350 nm (3.54 eV) via Sb^{3+} doping, which is assigned to the energy band originating from the Sb^{3+} ion.[16] It is remarkable that the absorption wavelength of 300−450 nm is enhanced with the increasing Sb^{3+}-doping content. Crystal samples with different Sb^{3+}-doping concentrations exhibit approximate PL peaks, as shown in Figure S2. Therefore, the sample with doping concentration of 5% Sb^{3+} was chosen to make further analysis. The PLE spectrum is located at 300−400 nm, which coincides with the absorption spectrum, indicating that the electron of the ground state was excited into the higher energy level of Sb^{3+} ions directly (Figure 2b). Under 340 nm excitation, the emission band at 580 nm with a full width at half maxima (fwhm) of 135 nm and a large Stokes shift of 240 nm has been monitored as well as a PLQY of 95.5% (Table S2). In comparison, the pristine $Cs_2InCl_5·H_2O$ showed no PL at a different excitation wavelength. The strongly localized 0D structure and the doping of Sb^{3+} to form the highly localized excitons in $Cs_2InCl_5·H_2O:Sb^{3+}$ crystal, as discussed below, is key to obtain intense yellow emission with such a high PLQY upon UV light irradiation (Figure 2c).

To reveal the underlying mechanism of the broadband emission, time-resolved PL (TRPL) spectra were measured. The average decay lifetime is determined to be 3.86 μs, which is composed of 1.51 μs (9.7%) and 4.1 μs (90.3%), respectively, indicating the existence of two emission behaviors (Figure S3). According to previous reports, the short- and long-decay time may be related to spin-triplet excited states transitions of $^3P_1 \rightarrow {}^1S_0$ and $^3P_0 \rightarrow {}^1S_0$, respectively.[33] To rule out the possibility of defect-induced emission,[22] the excitation power density-dependent PL intensity had been measured. As shown in Figure S4, the PL intensity of the emission is linearly dependent on the excitation power density. This suggests that the broadband emission is not from defects that will exhibit a saturated intensity upon such high excitation power density. However, the fitting seems not perfectly linear, and the extrinsic STEs could explain such evolution, as discussed below. Moreover, decay time of microsecond, together with the large Stokes shift and broadband emission, are the characteristics of STEs emission, suggesting that the broadband emission in $Cs_2InCl_5·H_2O:Sb^{3+}$ is the result of the radiative recombination of STEs.[25]

To further unveil the origin of the broadband emission behavior in $Cs_2InCl_5·H_2O:Sb^{3+}$ crystals, PL spectra excited at different wavelengths were measured. As shown in Figure S5a, no significant shift is found in PL spectra with excitation wavelength varying from 320 to 360 nm. The independent PLE spectra of different emission wavelengths also confirm that the yellow emission stem from the same excited state (Figure S5b). Next, PL measurements were carried out at a low temperature (80 K). As shown in Figure 3a, PL spectra shrink narrower at 80 K, which is attributed to the reduction of thermally populated vibrational states at low temperature,[34] and an additional PLE peak appeared, indicating the changing

https://dx.doi.org/10.1021/acs.chemmater.0c01708
Chem. Mater. 2020, 32, 5327−5334

of emission states. The PLE band 280 nm should be assigned to the $^1S_0-^1P_1$ transition and the triplet band 340 nm should be attributed to the $^1S_0-^3P_1$ transition.[16,35,36] Therefore, the effect of low temperature on luminescence can be shown by the consecutive PL/PLE correlation maps at 80 K (Figure 3b). Only EM1 (peaking at 580 nm) was displayed when the excitation wavelength varies from 320−340 nm and both EM1 and EM2 (peaking at 450 nm) were observed upon excitation wavelength from 260−300 nm. This characteristic phenomenon coincides with the unique singlet and triplet emission of ns^2 emission centers, as reported previously.[16,37,38] For the ns^2 ion, the ground state is named as $^1S_0$ and the excited states split into four energy levels $^1P_1$ and ^3P_n (n = 0, 1, 2), which are defined as singlet and triplet states, respectively. The transitions of $^1S_0 \rightarrow {}^3P_1$ or $^1S_0 \rightarrow {}^1P_1$ are parity-allowed because of spin−orbit coupling. The singlet and triplet radiation processes are further proved by the decay lifetimes, as shown in Figure 3c with lifetime of 8 ns of EM2 and microseconds of EM1, respectively.

The temperature-dependent PL spectra were measured upon excitation wavelengths of 340 and 280 nm. As shown in Figure 3d, under 340 nm excitation, only EM1 appeared with temperature changing from 80 to 290 K. Upon excitation at 280 nm, both peaks were observed, but the EM2 disappeared gradually with the increase of temperature (Figure S6). One possible reason is that higher temperatures will provide more thermal energy to overcome potential barriers between singlet states and triplet states, which will promote the intersystem crossing (ISC) process and eventually lead to the transition of electrons from singlet states to triplet states. The temperature-dependent PL intensity and fwhm (excitation at 340 nm) are shown in Figures S6 and 3e, respectively. The activation energy (E_a) can be calculated by the following eq 1

$$I(T) = \frac{I_0}{1 + A\exp\left(-\frac{E_a}{k_B T}\right)} \tag{3}$$

where $I(T)$ and I_0 are the integrated PL intensity at temperature T and 0 K, and k_B is the Boltzmann constant. The activation energy E_a = 136.95 meV is higher than that of other 3D perovskites, which is beneficial to radiative recombination.[39,40] The relationship between fwhm and temperature can be fitted by the following eq 2.

$$\text{fwhm} = 2.36\sqrt{S}\,\hbar\omega_{\text{phonon}}\sqrt{\coth\frac{\hbar\omega_{\text{phonon}}}{2k_B T}} \tag{4}$$

One can calculate the Huang−Rhys factor (S) of 32.28 and the phonon frequency ($\hbar\omega_{\text{phonon}}$) of 23.57 meV, respectively. The Huang−Rhys factor of $Cs_2InCl_5{\cdot}H_2O{:}Sb^{3+}$ is much higher than most luminescent materials, and the Huang−Rhys factors of different perovskites have been listed in Table S3,[22,41−45] which illustrate that electron-phonon coupling effect is closely related to lattice vibration and it is easy to form STEs in $Cs_2InCl_5{\cdot}H_2O{:}Sb^{3+}$. The photoexcitation radiation process for $Cs_2InCl_5{\cdot}H_2O{:}Sb^{3+}$ are shown in Figure 3f. Upon high energy photoexcitation (280 nm), the electrons transfer to the singlet state where a part of them relax to the ground state with EM2, while others undergo an ISC process to the triplet states, leading to EM1 emission. Upon low energy photoexcitation (340 nm), the EM1 emission is also attributed to triplet excitonic recombination. The formation of STEs are related to the 0D crystal structure and the nature of halide perovskite, thus leading to broad emission and large Stokes shift.[23,46]

To elucidate the optical properties and PL mechanisms of $Cs_2InCl_5{\cdot}H_2O{:}Sb^{3+}$, the electronic band structure and densities of states were calculated based on DFT calculations. The $Cs_2InCl_5{\cdot}H_2O$ possesses a calculated band gap of 3.4 eV (Figure 4a), and the value of $Cs_2InCl_5{\cdot}H_2O{:}Sb^{3+}$ has declined to 2.7 eV (Figure 4b), which indicate that band gap would be reduced by Sb^{3+} doping. For $Cs_2InCl_5{\cdot}H_2O$, the valence band maximum comprise the Cl-3p state and the conduction band minimum has a mixed In-5s and Cl-3p character, as shown in Figure 4c. Analysis of $Cs_2InCl_5{\cdot}H_2O{:}Sb^{3+}$ shows that the Sb 5s orbitals exclusively occupies the top of the valence bands, and the bottom of the conduction bands is dominantly occupied by Sb 5s, In 5s, and Cl-3p orbitals (Figure 4d). However, the orbitals of indium and chloride keep almost unchanged. The calculation results demonstrate that the PL mechanism is affected by the dopants sites, consequently leading to the broadband yellow emission.

The same method can be easily extended to synthesize $Cs_2InX_5{\cdot}H_2O{:}Sb^{3+}$ crystals with different halogen atoms, where X represents mixed halogen compositions. The crystal structures of $Cs_2InX_5{\cdot}H_2O{:}Sb^{3+}$ (X = Cl/Br/I) are the same as $Cs_2InCl_5{\cdot}H_2O$ as discussed above except for that the iodide-based end member cannot be synthesized. The XRD patterns are shown in Figure 5a. All samples are of the pure phase and the diffraction peaks at 15° shift to lower degrees with the exchange of halogen from chlorine to bromine, and partial iodine. As shown in Figure 5b, the PL spectra of $Cs_2InX_5{\cdot}H_2O{:}Sb^{3+}$ can be finely tuned from 580 to 660 nm by varying the composition of halogens. The $Cs_2InCl_5{\cdot}H_2O{:}Sb^{3+}$, $Cs_2InBr_5{\cdot}H_2O{:}Sb^{3+}$, and $Cs_2InBr_3I_2{\cdot}H_2O{:}Sb^{3+}$ demonstrated different emission peaks at 580, 630, and 660 nm, respectively. As shown in Figure S8, the PL intensity of $Cs_2InBr_5{\cdot}H_2O{:}Sb^{3+}$ is linearly dependent on the excitation power density, which is similar to that of $Cs_2InCl_5{\cdot}H_2O{:}Sb^{3+}$, further confirming the extrinsic STEs emission centers. Various crystals show emission colors from yellow to red under UV light and the CIE coordinates can be tuned obviously (Figure 5c). The PLQYs of $Cs_2InX_5{\cdot}H_2O{:}Sb^{3+}$ are summarized in Table S4. The decay lifetime of various $Cs_2InX_5{\cdot}H_2O{:}Sb^{3+}$ was determined to be microseconds and decreased gradually from chloride to bromide, as shown in Figure 5d.

We further studied the stability of the as-prepared crystals because it was intensely relevant to the application. First, we focus on the effect of the bound water molecule in $Cs_2InX_5{\cdot}H_2O{:}Sb^{3+}$ on the PL properties. The proof of the water was confirmed by FTIR spectroscopy and thermogravimetry analysis (TGA). As shown in Figure S9, the absorption from 1500 to 1600 cm^{-1} belong to H−O bending vibration (δ_{H-O}) and the absorption from 3000 to 3600 cm^{-1} is attributed to H−O stretching vibration (ν_{H-O}) of bound water for $Cs_2InCl_5{\cdot}H_2O{:}Sb^{3+}$ and $Cs_2InBr_5{\cdot}H_2O{:}Sb^{3+}$, also consistent with the recent report.[20] The TGA was carried out for both chloride and bromide samples at the nitrogen atmosphere. Consequently, the $Cs_2InCl_5{\cdot}H_2O{:}Sb^{3+}$ begins to lose the water molecule at 160 °C, which is higher than that of $Cs_2InBr_5{\cdot}H_2O{:}Sb^{3+}$ around 120 °C (Figure S10), indicating that $Cs_2InCl_5{\cdot}H_2O{:}Sb^{3+}$ have better structural stability. Interestingly, the dehydrated sample shows similar PL spectra with that of pristine $Cs_2InCl_5{\cdot}H_2O{:}Sb^{3+}$ (the inset of Figure 5a). The temperature-dependent PL measurement of $Cs_2InCl_5{\cdot}H_2O{:}Sb^{3+}$ from RT to 500 K in the air also exhibit brilliant

https://dx.doi.org/10.1021/acs.chemmater.0c01708
Chem. Mater. 2020, 32, 5327−5334

thermal stability and the emission intensity, and the intensities keep about 70% at 425 K compared with the initial intensity at RT (Figure 6a).

The broadband emission with high PLQY, as well as good thermal stability, makes the lead-free $Cs_2InCl_5·H_2O:Sb^{3+}$ potential materials for WLEDs applications. Thus, we fabricated a WLED with the yellow-emitting $Cs_2InCl_5·H_2O:Sb^{3+}$ powders and blue phosphor $BaMgAl_{10}O_{17}:Eu^{2+}$ in epoxy resin, then covering the mixture on a commercial 365 nm UV chip. Figure 6b shows the PL spectra of the WLED device under a current of 20 mA. The CIE of the obtained WLED is (0.3576, 0.3547), corresponding to a color-rendering index (R_a) of 86 and the white light CCT of 4556 K (Figure 6c). These results indicate that the inorganic lead-free 0D perovskites have prospective applications in solid-state lighting. In addition, we also use the $Cs_2InBr_5·H_2O:Sb^{3+}$ powders to make present patterns by screen printing (Figure 6d). The powders were mixed with epoxy resin, and thus, the high-resolution patterns such as the quick response (QR) code and other fluorescence images can be printed by using this kind of luminescence materials. It is found that $Cs_2InX_5·H_2O:Sb^{3+}$ with highly efficient and tunable emission enable its potential application in high-resolution images and fluorescent signs.

CONCLUSIONS

In conclusion, the lead-free all-inorganic 0D $Cs_2InCl_5·H_2O$ crystal was reported with an extrinsic STEs emission via Sb^{3+} ion doping. A broadband yellow emission has been performed with a long lifetime (3.86 μs) and a large Stokes shift around 240 nm. Experimental studies by the combined steady/transient state fluorescence spectral properties reveal that a strong electron phonon coupling in the soft crystal structure, as further altered by Sb^{3+} doping, results in the formation of STE emission. The 0D structure and highly localized excitons render $Cs_2InCl_5·H_2O:Sb^{3+}$ a high PLQY of 95.5%, as also discussed by the theoretical analysis. PL spectra of $Cs_2InX_5·H_2O:Sb^{3+}$ crystals can be tuned from 580 to 660 nm with the substitution of halogen from chlorine and bromine to iodine. Highly efficient and tunable emission in $Cs_2InX_5·H_2O:Sb^{3+}$, as well as an excellent thermal stability, motivate its diverse applications in WLEDs and high-resolution fluorescent images, and such fully inorganic, thermally robust, and bright emitters will find new applications, which were also anticipated.

ASSOCIATED CONTENT

Supporting Information

The Supporting Information is available free of charge at https://pubs.acs.org/doi/10.1021/acs.chemmater.0c01708.

Main parameters of processing and refinement; optical properties of $Cs_2InX_5·H_2O:Sb^{3+}$ samples; XPS spectra; PL emission spectra; luminescent decay times; PL intensity of $Cs_2InX_5·H_2O:Sb^{3+}$ (X = Cl, Br) as a function of excitation power; consecutive PL/temperature correlation maps; Arrhenius plot of integrated PL intensity versus the reciprocal of temperature ($1/T$); and FTIR spectra and TGA curves of $Cs_2InX_5·H_2O:Sb^{3+}$ (X = Cl, Br) samples (PDF).

AUTHOR INFORMATION

Corresponding Author

Zhiguo Xia − *The Beijing Municipal Key Laboratory of New Energy Materials and Technologies, School of Materials Science and Engineering, University of Science and Technology Beijing, Beijing 100083, China; The State Key Laboratory of Luminescent Materials and Devices, Guangdong Provincial Key Laboratory of Fiber Laser Materials and Applied Techniques, School of Materials Science and Technology, South China University of Technology, Guangzhou 510640, China;* orcid.org/0000-0002-9670-3223; Email: xiazg@scut.edu.cn

Authors

Yuyu Jing − *The Beijing Municipal Key Laboratory of New Energy Materials and Technologies, School of Materials Science and Engineering, University of Science and Technology Beijing, Beijing 100083, China*

Ying Liu − *The Beijing Municipal Key Laboratory of New Energy Materials and Technologies, School of Materials Science and Engineering, University of Science and Technology Beijing, Beijing 100083, China*

Xingxing Jiang − *Technical Institute of Physics and Chemistry, Chinese Academy of Sciences, Beijing 100190, China*

Maxim S. Molokeev − *Laboratory of Crystal Physics, Kirensky Institute of Physics, Federal Research Center KSC SB RAS, Krasnoyarsk 660036, Russia; Siberian Federal University, Krasnoyarsk 660041, Russia; Department of Physics, Far Eastern State Transport University, Khabarovsk 680021, Russia*

Zheshuai Lin − *Technical Institute of Physics and Chemistry, Chinese Academy of Sciences, Beijing 100190, China; University of Chinese Academy of Sciences, Beijing 100049, China;* orcid.org/0000-0002-9829-9893

Complete contact information is available at: https://pubs.acs.org/10.1021/acs.chemmater.0c01708

Author Contributions

$^{\nabla}$Y.J. and Y.L. are contributed equally.

Notes

The authors declare no competing financial interest.

ACKNOWLEDGMENTS

This work is supported by the National Natural Science Foundation of China (51961145101, 51972118, and 51722202), Fundamental Research Funds for the Central Universities (FRFTP-18-002C1), Guangzhou Science & Technology Project (202007020005), Guangdong Provincial Science &Technology Project (2018A050506004), and the Local Innovative and Research Teams Project of Guangdong Pearl River Talents Program (2017BT01X137). This work is also funded by RFBR according to the research project no. 19-52-80003.

REFERENCES

(1) Akkerman, Q. A.; Rainò, G.; Kovalenko, M. V.; Manna, L. Genesis, Challenges and Opportunities For Colloidal Lead Halide Perovskite Nanocrystals. *Nat. Mater.* **2018**, *17*, 394−405.

(2) Protesescu, L.; Yakunin, S.; Bodnarchuk, M. I.; Krieg, F.; Caputo, R.; Hendon, C. H.; Yang, R. X.; Walsh, A.; Kovalenko, M. V. Nanocrystals of Cesium Lead Halide Perovskites ($CsPbX_3$, X = Cl, Br, and I): Novel Optoelectronic Materials Showing Bright Emission with Wide Color Gamut. *Nano Lett.* **2015**, *15*, 3692−3696.

(3) Wu, Y.; Li, X.; Zeng, H. Highly Luminescent and Stable Halide Perovskite Nanocrystals. *ACS Energy Lett.* **2019**, *4*, 673−681.

(4) Fan, Q.; Biesold-McGee, G. V.; Xu, Q.; Pan, S.; Peng, J.; Ma, J.; Lin, Z. Lead-Free Halide Perovskite Nanocrystals: Crystal Structures,

Synthesis, Stabilities, and Optical Properties. *Angew. Chem., Int. Ed. Engl.* **2020**, *59*, 1030−1046.
(5) Xiao, Z.; Song, Z.; Yan, Y. From Lead Halide Perovskites to Lead-Free Metal Halide Perovskites and Perovskite Derivatives. *Adv. Mater.* **2019**, *31*, 1803792.
(6) Xia, Z.; Poeppelmeier, K. R. Chemistry-Inspired Adaptable Framework Structures. *Acc. Chem. Res.* **2017**, *50*, 1222−1230.
(7) Igbari, F.; Wang, Z. K.; Liao, L. S. Progress of Lead-Free Halide Double Perovskites. *Adv. Energy Mater.* **2019**, *9*, 1803150.
(8) Tran, T. T.; Panella, J. R.; Chamorro, J. R.; Morey, J. R.; McQueen, T. M. Designing Indirect-direct Bandgap Transitions in Double Perovskites. *Mater. Horiz.* **2017**, *4*, 688−693.
(9) Zhou, J.; Xia, Z.; Molokeev, M. S.; Zhang, X.; Peng, D.; Liu, Q. Composition Design, Optical Gap and Stability Investigations of Lead-free Halide Double Perovskite $Cs_2AgInCl_6$. *J. Mater. Chem. A* **2017**, *5*, 15031−15037.
(10) Yang, B.; Mao, X.; Hong, F.; Meng, W.; Tang, Y.; Xia, X.; Yang, S.; Deng, W.; Han, K. Lead-Free Direct Band Gap Double-Perovskite Nanocrystals with Bright Dual-Color Emission. *J. Am. Chem. Soc.* **2018**, *140*, 17001−17006.
(11) Liu, Y.; Jing, Y.; Zhao, J.; Liu, Q.; Xia, Z. Design Optimization of Lead-Free Perovskite $Cs_2AgInCl_6$:Bi Nanocrystals with 11.4% Photoluminescence Quantum Yield. *Chem. Mater.* **2019**, *31*, 3333−3339.
(12) Yang, B.; Chen, J.; Hong, F.; Mao, X.; Zheng, K.; Yang, S.; Li, Y.; Pullerits, T.; Deng, W.; Han, K. Lead-Free, Air-Stable All-Inorganic Cesium Bismuth Halide Perovskite Nanocrystals. *Angew. Chem., Int. Ed. Engl.* **2017**, *56*, 12471−12475.
(13) Zhang, J.; Yang, Y.; Deng, H.; Farooq, U.; Yang, X.; Khan, J.; Tang, J.; Song, H. High Quantum Yield Blue Emission from Lead-Free Inorganic Antimony Halide Perovskite Colloidal Quantum Dots. *ACS Nano* **2017**, *11*, 9294−9302.
(14) Xing, G.; Kumar, M. H.; Chong, W. K.; Liu, X.; Cai, Y.; Ding, H.; Asta, M.; Grätzel, M.; Mhaisalkar, S.; Mathews, N.; Sum, T. C. Solution-Processed Tin-Based Perovskite for Near-Infrared Lasing. *Adv. Mater.* **2016**, *28*, 8191−8196.
(15) Jun, T.; Sim, K.; Iimura, S.; Sasase, M.; Kamioka, H.; Kim, J.; Hosono, H. Lead-Free Highly Efficient Blue-Emitting $Cs_3Cu_2I_5$ with 0D Electronic Structure. *Adv. Mater.* **2018**, *30*, 1804547.
(16) Jing, Y.; Liu, Y.; Zhao, J.; Xia, Z. Sb^{3+} Doping-Induced Triplet Self-Trapped Excitons Emission in Lead-Free Cs_2SnCl_6 Nanocrystals. *J. Phys. Chem. Lett.* **2019**, *10*, 7439−7444.
(17) Lin, R.; Guo, Q.; Zhu, Q.; Zhu, Y.; Zheng, W.; Huang, F. All-Inorganic $CsCu_2I_3$ Single Crystal with High-PLQY (∼15.7%) Intrinsic White-Light Emission via Strongly Localized 1D Excitonic Recombination. *Adv. Mater.* **2019**, *46*, 1905079.
(18) Zhou, G.; Su, B.; Huang, J.; Zhang, Q.; Xia, Z. Broad-band Emission in Metal Halide Perovskites: Mechanism, Materials, and Applications. *Mater. Sci. Eng. R Rep.* **2020**, *141*, 100548.
(19) Piszczek, P.; Grodzicki, A.; Engelen, B. Infrared and Raman Studies of Water Molecule Normal Vibrations in Crystalline Hydrates Which Form the Chain Structures. *J. Mol. Struct.* **2003**, *646*, 45−54.
(20) Zhou, L.; Liao, J. F.; Huang, Z. G.; Wei, J. H.; Wang, X. D.; Li, W. G.; Chen, H. Y.; Kuang, D. B.; Su, C. Y. A Highly Red-Emissive Lead-Free Indium-Based Perovskite Single Crystal for Sensitive Water Detection. *Angew. Chem., Int. Ed. Engl.* **2019**, *58*, 5277−5281.
(21) Solans, X.; Moron, M. C.; Palacio, F. Structures of $Rb_2[InCI_5(H_2O)]$ and $Cs_2[InCI_5(H_2O)]$. *Acta Crystallogr. Sect. C Cryst. Struct. Commun.* **1988**, *44*, 965−967.
(22) Luo, J.; Wang, X.; Li, S.; Liu, J.; Guo, Y.; Niu, G.; Yao, L.; Fu, Y.; Gao, L.; Dong, Q.; Zhao, C.; Leng, M.; Ma, F.; Liang, W.; Wang, L.; Jin, S.; Han, J.; Zhang, L.; Etheridge, J.; Wang, J.; Yan, Y.; Sargent, E. H.; Tang, J. Efficient and Stable Emission of Warm-white Light from Lead-free Halide Double Perovskites. *Nature* **2018**, *563*, 541−545.
(23) Smith, M. D.; Karunadasa, H. I. White-Light Emission from Layered Halide Perovskites. *Acc. Chem. Res.* **2018**, *51*, 619−627.
(24) Zhou, L.; Liao, J. F.; Huang, Z. G.; Wei, J. H.; Wang, X. D.; Chen, H. Y.; Kuang, D. B. Intrinsic Self-Trapped Emission in 0D Lead-Free $(C_4H_{14}N_2)_2In_2Br_{10}$ Single Crystal. *Angew. Chem., Int. Ed. Engl.* **2019**, *58*, 15435−15440.
(25) Li, S.; Luo, J.; Liu, J.; Tang, J. Self-Trapped Excitons in All-Inorganic Halide Perovskites: Fundamentals, Status, and Potential Applications. *J. Phys. Chem. Lett.* **2019**, *10*, 1999−2007.
(26) Locardi, F.; Sartori, E.; Buha, J.; Zito, J.; Prato, M.; Pinchetti, V.; Zaffalon, M. L.; Ferretti, M.; Brovelli, S.; Infante, I.; De Trizio, L.; Manna, L. Emissive Bi-Doped Double Perovskite $Cs_2Ag_{1-x}Na_xInCl_6$ Nanocrystals. *ACS Energy Lett.* **2019**, *4*, 1976−1982.
(27) Yu, J.; Kong, J.; Hao, W.; Guo, X.; He, H.; Leow, W. R.; Liu, Z.; Cai, P.; Qian, G.; Li, S.; Chen, X.; Chen, X. Broadband Extrinsic Self-Trapped Exciton Emission in Sn-Doped 2D Lead-Halide Perovskites. *Adv. Mater.* **2019**, *31*, 1806385.
(28) Clark, S. J.; Segall, M. D.; Pickard, C. J.; Hasnip, P. J.; Probert, M. I. J.; Refson, K.; Payne, M. C. First Principles Methods Using CASTEP. *Z. Kristallogr.* **2005**, *220*, 567−570.
(29) Ceperley, D. M.; Alder, B. J. Ground State of the Electron Gas by a Stochastic Method. *Phys. Rev. Lett.* **1980**, *45*, 566−569.
(30) Bruker, Topas. *General Profile and Structure Analysis Software for Powder Diffraction Data*, version 4; Bruker AXS: Karlsruhe: Germany, 2008.
(31) Guo, S.; Wang, Y.; Wang, C.; Tang, Z.; Zhang, J. Large Spin-orbit Splitting in the Conduction Band of Halogen (F, Cl, Br, and I) Doped Monolayer WS_2 with Spin-orbit Coupling. *Phys. Rev. B* **2017**, *96*, 245305.
(32) Zhang, X.; Wang, H.; Hu, Y.; Pei, Y.; Wang, S.; Shi, Z.; Colvin, V. L.; Wang, S.; Zhang, Y.; Yu, W. W. Strong Blue Emission from Sb^{3+}-Doped Super Small $CsPbBr_3$ Nanocrystals. *J. Phys. Chem. Lett.* **2019**, *10*, 1750−1756.
(33) Kang, F.; Zhang, H.; Wondraczek, L.; Yang, X.; Zhang, Y.; Lei, D. Y.; Peng, M. Band-Gap Modulation in Single Bi^{3+}-Doped Yttrium−Scandium−Niobium Vanadates for Color Tuning over the Whole Visible Spectrum. *Chem. Mater.* **2016**, *28*, 2692−2703.
(34) Zhou, C.; Lin, H.; Tian, Y.; Yuan, Z.; Clark, R.; Chen, B.; van de Burgt, L. J.; Wang, J. C.; Zhou, Y.; Hanson, K.; Meisner, Q. J.; Neu, J.; Besara, T.; Siegrist, T.; Lambers, E.; Djurovich, P.; Ma, B. Luminescent Zero-dimensional Organic Metal Halide Hybrids with Near-unity Quantum Efficiency. *Chem. Sci.* **2018**, *9*, 586−593.
(35) Ranfagni, A.; Mugnai, D.; Bacci, M.; Viliani, G.; Fontana, M. P. The Optical Properties of Thallium-like Impurities in Alkali-halide Crystals. *Adv. Phys.* **1983**, *32*, 823−905.
(36) Wen, F.; Chen, J.; Moon, J.-H.; Kim, J. H.; Niu, J.; Li, W. Hydrothermal Synthesis and Luminescent Properties of Sb^{3+}-doped $Sr_3(PO_4)_2$. *J. Solid State Chem.* **2004**, *177*, 3114−3118.
(37) Li, Z.; Li, Y.; Liang, P.; Zhou, T.; Wang, L.; Xie, R.-J. Dual-Band Luminescent Lead-Free Antimony Chloride Halides with Near-Unity Photoluminescence Quantum Efficiency. *Chem. Mater.* **2019**, *31*, 9363−9371.
(38) Morad, V.; Shynkarenko, Y.; Yakunin, S.; Brumberg, A.; Schaller, R. D.; Kovalenko, M. V. Disphenoidal Zero-Dimensional Lead, Tin, and Germanium Halides: Highly Emissive Singlet and Triplet Self-Trapped Excitons and X-ray Scintillation. *J. Am. Chem. Soc.* **2019**, *141*, 9764−9768.
(39) Yang, H.; Zhang, Y.; Pan, J.; Yin, J.; Bakr, O. M.; Mohammed, O. F. Room-Temperature Engineering of All-Inorganic Perovskite Nanocrsytals with Different Dimensionalities. *Chem. Mater.* **2017**, *29*, 8978−8982.
(40) Zhou, L.; Liao, J. F.; Huang, Z. G.; Wei, J. H.; Wang, X. D.; Chen, H. Y.; Kuang, D. B. Intrinsic Self-Trapped Emission in 0D Lead-Free $(C_4H_{14}N_2)_2In_2Br_{10}$ Single Crystal. *Angew. Chem., Int. Ed. Engl.* **2019**, *58*, 15435−15440.
(41) Türck, V.; Rodt, S.; Stier, O.; Heitz, R.; Engelhardt, R.; Pohl, U. W.; Bimberg, D.; Steingrüber, R. Effect of Random Field Fluctuations on Excitonic Transitions of Individual CdSe Quantum Dots. *Phys. Rev. B: Condens. Matter Mater. Phys.* **2000**, *61*, 9944−9947.
(42) Zhao, H.; Kalt, H. Energy-dependent Huang-Rhys Factor of Free Excitons. *Phys. Rev. B: Condens. Matter Mater. Phys.* **2003**, *68*, 125309.

https://dx.doi.org/10.1021/acs.chemmater.0c01708
Chem. Mater. 2020, 32, 5327−5334

(43) McCall, K. M.; Stoumpos, C. C.; Kostina, S. S.; Kanatzidis, M. G.; Wessels, B. W. Strong Electron−Phonon Coupling and Self-Trapped Excitons in the Defect Halide Perovskites $A_3M_2I_9$ (A = Cs, Rb; M = Bi, Sb). *Chem. Mater.* **2017**, *29*, 4129−4145.
(44) Lao, X.; Yang, Z.; Su, Z.; Wang, Z.; Ye, H.; Wang, M.; Yao, X.; Xu, S. Luminescence and Thermal Behaviors of Free and Trapped Excitons in Cesium Lead Halide Perovskite Nanosheets. *Nanoscale* **2018**, *10*, 9949−9956.
(45) Yang, B.; Yin, L.; Niu, G.; Yuan, J. H.; Xue, K. H.; Tan, Z.; Miao, X. S.; Niu, M.; Du, X.; Song, H.; Lifshitz, E.; Tang, J. Lead-Free Halide Rb_2CuBr_3 as Sensitive X-Ray Scintillator. *Adv. Mater.* **2019**, *31*, 1904711.
(46) Benin, B. M.; Dirin, D. N.; Morad, V.; Wörle, M.; Yakunin, S.; Rainò, G.; Nazarenko, O.; Fischer, M.; Infante, I.; Kovalenko, M. V. Highly Emissive Self-Trapped Excitons in Fully Inorganic Zero-Dimensional Tin Halides. *Angew. Chem., Int. Ed. Engl.* **2018**, *57*, 11329−11333.

■ NOTE ADDED AFTER ASAP PUBLICATION

This paper was published ASAP on May 29, 2020, with incorrect Figure 3. The corrected version was reposted on June 2, 2020.

https://dx.doi.org/10.1021/acs.chemmater.0c01708
Chem. Mater. 2020, 32, 5327−5334